Young's modulus and internal friction in metallic glass alloys from 1.5 to 300 K

M. Barmatz and H. S. Chen
Bell Laboratories, Murray Hill, New Jersey 07974
(Received 10 January 1974)

An investigation of the acoustic properties of metallic glass alloys has been carried out in the temperature range 1.5–300 K. The Young's modulus and internal friction were measured in the frequency range 0.1–3 kHz using a vibrating-reed technique. The Young's modulus of the alloys investigated experienced large increases of from 26% to 39% after crystallization. The internal friction in the amorphous and crystalline phases of the binary alloys $Pd_{0.81}Si_{0.19}$ is consistent with a thermoelastic relaxation process. Low-temperature anomalies in the damping and dispersion of multicomponent nickel and iron alloys were observed superimposed on the thermoelastic loss. The low-temperature measurements in the amorphous phase of $Fe_{0.74}P_{0.16}C_{0.05}Al_{0.03}Si_{0.02}$ were characterized by a broad distribution of relaxation times. This distribution is asymmetric, corresponding to excess damping and dispersion at temperatures below the internal-friction maximum. Crystallization removes the asymmetry and the crystalline measurements fit a log-normal distribution of relaxation times with $\beta \simeq 13$. A temperature-dependent relaxation strength such as that proposed by Scott and MacCrone explains the main features of the observed low-temperature asymmetry.

In recent years, several amorphous metallic alloys[1,2] have been prepared by rapid-quenching techniques. At the present time, bulk samples of these materials are difficult to produce and information regarding their general properties are limited. Measurements of the mechanical behavior of amorphous metals[3–9] have indicated that the amorphous state is characterized by an elastic softening relative to its crystalline counterpart. Some of these alloys also exhibit a large anharmonicity in both the amorphous and crystalline phases.[10] However, little information is available on the temperature dependence of the mechanical properties of these amorphous metallic alloys.

In the present investigation we present internal-friction and Young's-modulus measurements in the amorphous and crystalline states of metallic alloys over the temperature range 1.5–300 K. The measurements were carried out in the frequency range 0.1–3 kHz using a vibrating-reed technique. The alloys investigated were $Pd_{0.81}Si_{0.19}$, $Fe_{0.74}P_{0.16}C_{0.05}Al_{0.03}Si_{0.02}$, $Fe_{0.75}P_{0.16}Si_{0.06}Al_{0.03}$, and $Ni_{0.74}P_{0.16}B_{0.07}Al_{0.03}$. Measurements of the change in Young's modulus upon crystallization of several metallic alloys are compared to theoretical predictions.

Zener's theory of thermoelastic relaxation is shown to account for the internal friction in the amorphous and crystalline phases of $Pd_{0.81}Si_{0.19}$. From an analysis of the measurements, we determine the magnitude and temperature dependence of the diffusivity and thermal conductivity. In the multicomponent iron and nickel alloys, in addition to the thermoelastic loss, there is a broad low-temperature internal-friction maximum in the amorphous phase. The low-temperature internal friction and associated dispersion are analyzed using a broad spectrum of relaxation times. The low-temperature damping is also present in the crystalline phase.

I. THEORY

A. Internal friction

A well-known relaxation mechanism in thin reeds is the thermoelastic loss, first described by Zener.[11] During flexural vibration one side of the reed is compressed and heats, while the opposite side is extended and cools. In this process, energy is lost from the sound wave, due to heat flow from warmer to cooler regions of the reed. The characteristic time for heat to flow from the heated to cooled side of a rectangular reed is

$$\tau_R(T) = (t/\pi)^2 D^{-1}(T), \tag{1}$$

where t is the sample thickness and $D = \lambda/C_p$ is the thermal diffusivity, with λ and C_p being the thermal conductivity and isobaric specific heat, respectively. Zener showed[11] that to a good approximation ($\lesssim 2\%$) the internal friction and Young's-modulus dispersion could be represented by the single relaxation expressions

$$Q^{-1}(\omega, T) = A[\omega\tau_R/(1+\omega^2\tau_R^2)], \tag{2}$$

$$[E(\omega, T) - E_T(T)]/E_T(T) = A[\omega^2\tau_R^2/(1+\omega^2\tau_R^2)], \tag{3}$$

where $E_T(T)$ is the isothermal Young's modulus. The relaxation strength, A, is given by

$$A = TE_T\alpha^2/C_p, \tag{4}$$

where α is the linear thermal expansion coefficient. For $\omega\tau_R \ll 1$, the heat generated by flexural motion has time to flow across the reed within half a sound period and we have isothermal propagation. For higher frequencies where $\omega\tau_R \gg 1$, the propagation is adiabatic. In the present investigation, measurements covered both the adiabatic and isotherm-

al regimes. For most materials, the thermoelastic-relaxation process becomes unimportant at low temperatures, since the relaxation strength, Eq. (4), decreases sharply as $T \to 0$ K. This is not the case, however, for materials which have low-temperature phase transitions.[12]

Previous acoustic investigations of glasses[6,13] have revealed relaxation processes with a broad spectrum of relaxation times. To interpret these measurements it is usually convenient to introduce a relaxation time distribution function $\varphi(\tau)$ such that

$$Q^{-1} = \Delta \int_0^\infty \varphi(\tau)\omega\tau\, d\tau/(1+\omega^2\tau^2) \tag{5}$$

where Δ is a relaxation strength. In the present investigation, we have interpreted the low-temperature internal-friction measurements using a Gaussian distribution in $\ln\tau$ (log-normal distribution). The log-normal distribution function is defined by

$$\varphi(\tau)d\tau = (\beta\sqrt{\pi})^{-1} e^{-(z/\beta)^2} dz \tag{6}$$

where $z = \ln(\tau/\tau_m)$. τ_m is the mean value of the relaxation time and β is a parameter which measures the width of the distribution. A single relaxation time corresponds to $\beta = 0$. The higher the value of β the larger is the spectrum of relaxation times. Numerical calculations of the internal friction based on the log-normal distribution of relaxation times are available[14,15] as a function of β.

B. Young's modulus

Recently, a theoretical analysis of the mechanical properties of amorphous materials was carried out by Weaire *et al.*[16] They used a quasicontinuum and discrete-atom model to calculate the difference in density, energy, bulk modulus, and shear modulus between the glass and crystalline phases. A theoretical estimate for the change in Young's modulus may be obtained from their results as follows. The relationship between the amorphous Young's modulus E, the shear modulus μ, and the bulk modulus B for a homogeneous solid is given by

$$E = 9B\mu/(\mu + 3B). \tag{7}$$

Using this equation, the change in modulus can be written in the form

$$\frac{\Delta E}{E} = \frac{\Delta\mu}{\mu}\left(1 - \frac{R}{R+3}\right) + \frac{\Delta B}{B}\left(1 - \frac{3}{R+3}\right), \tag{8}$$

with $R = \mu/B$. By assuming to a first approximation that no internal displacements take place, we obtain the simplifying relation $R = \frac{3}{5}$ between B and μ.[15] Substitution into Eq. (8) yields

$$\frac{\Delta E}{E} \simeq \frac{5}{6}\frac{\Delta\mu}{\mu} + \frac{1}{6}\frac{\Delta B}{B}. \tag{9}$$

Weaire *et al.* found that upon crystallization the shear and bulk moduli changed by $\Delta\mu/\mu \simeq 29\%$–$58\%$ and $\Delta B/B \simeq 4\%$–17%, respectively. Using these values in Eq. (9) leads to an expected Young's-modulus change $\Delta E/E \simeq 25\%$–51%.

II. EXPERIMENTAL

A. Technique

A squeeze-quenching technique[2] was used to prepare the amorphous alloys, except for $Ni_{0.76}P_{0.24}$.[17] The samples were in the form of thin reeds ~0.3 cm wide, ~1.8 cm long, and from 50 to 120 μm thick. The Young's modulus and internal friction were determined using a vibrating-reed method described previously.[18] Each specimen was clamped at one end between two stainless-steel plates and was free to vibrate at the other. Flectural vibrations were excited and detected with identical electrostatic transducers situated on either side of the free end. The flectural resonant frequency of the nth overtone for a clamped-free rectangular reed is[19]

$$f_n = \frac{\kappa}{2\pi}\left(\frac{k_n}{l}\right)^2 v_E, \tag{10}$$

where $\kappa = t/\sqrt{12}$ is the radius of gyration, and t and l are the reed thickness and length, respectively. The resonant frequency is directly proportional to the Young's-modulus velocity along the reed $v_E = (E/\rho)^{1/2}$, where E is the Young's modulus and ρ is the density. The constants k_n are 1.875, 4.694, 7.855, ... for the overtones $n = 1, 2, 3, \ldots$. The flexural resonances are not harmonic, the second-overtone frequency being 6.28 times the fundamental.

B. Apparatus

A schematic of the apparatus is shown in Fig. 1. An Au-Fe vs chromel thermocouple determined the sample temperature and was situated in one of the plates clamping the sample. The thermocouple and a heater (100-Ω carbon resistor), located in the other clamping plate, were part of a temperature controller which could regulate the sample temperature to better than 0.02 °K. The clamped sample was secured in a copper block containing the drive and receiver electrodes and the entire assembly was suspended by strings from a copper platform. The platform also served as the support for a heat shield whose temperature was controlled automatically. All measurements were carried out under equilibrium conditions at pressures less than 10^{-4} torr.

The receiver circuit is shown in Fig. 2(a). A bias voltage V_B was supplied across the receiver capacitor C_R through a large resistor (~50 MΩ).

The receiver capacitance (~0.2 pF) was small compared to the cable capacitance C_c (~100 pF) and this led to a substantial loss in the signal at the amplifier input. Limitations on the magnitude of the bias voltage, imposed by the electrostatic coupling discussed below, further reduced the received signal. To minimize the loading effect of the cable capacitance, a three-lead receiver configuration was employed using a guarded shield. This technique increased the detected signal by ~20 dB.

The close proximity of the drive and receiver electrodes lead to a large capacitive coupling. This coupling resulted in substantial pickup of the drive signal, which could saturate the detector electronics. A simple bridge circuit was employed to generate a reference signal at the detector which was equal in magnitude, but 180° out of phase, with the extraneous pickup signal. With this system the unwanted coupling signal could be nulled in the detector circuit.

C. Electrostatic coupling

For thin reeds, the flexural resonant frequency is a function of the receiver bias voltage. This frequency dependence may be quantitatively understood by considering the coupling between the electrostatic and mechanical systems. A schematic of the receiver transducer is shown in Fig. 2(b). We define the electrostatic energy to be zero at infinity

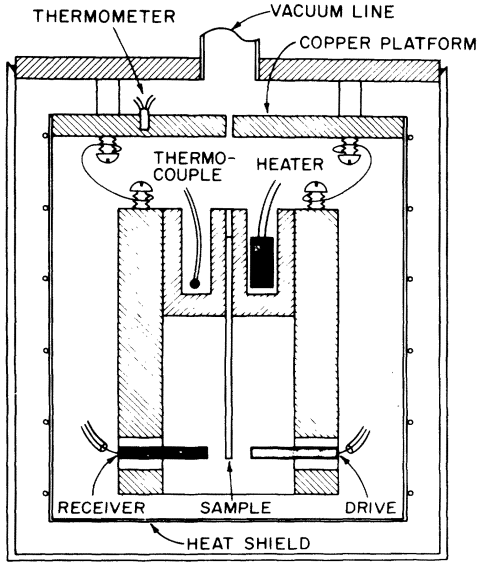

FIG. 1. Apparatus. Two stainless-steel blocks clamped the metallic sample. A heater and thermocouple, situated in the blocks, controlled the sample temperature. The clamped assembly was held by a copper housing containing the drive and receiver electrodes. A temperature-controlled heat shield surrounded the copper housing.

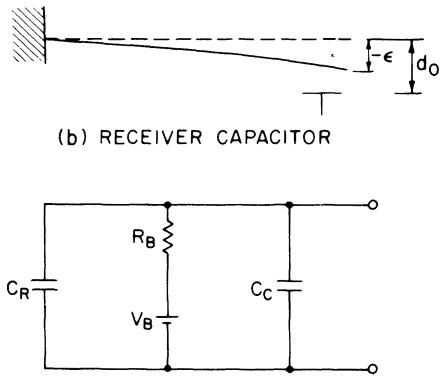

FIG. 2. (a) Receiver capacitance C_R was dc biased through a large resistor R_B. Bias voltages ranged from $V_B \simeq 5$ to 20 V. The loading effect of the cable capacitance C_c was minimized using a three-lead configuration with a guarded shield. (b) Schematic of receiver transducer. The dashed line represents the zero-biased sample position corresponding to a capacitance gap of d_0. A dc bias voltage V_B caused the reed to be displaced by $-\epsilon$ from its equilibrium position.

and assume the dc bias voltage V_B remains constant during the reed vibration. The total energy $\mathcal{E}_T$ of the vibrating reed is the sum of the mechanical and electrical contributions,

$$\mathcal{E}_T = \tfrac{1}{2} y\epsilon^2 - \tfrac{1}{2}(\epsilon_0 A V_B^2)/(d_0+\epsilon) \qquad (11)$$

where y is the mechanical bending modulus, ϵ is the reed displacement from its equilibrium position, and d_0 is the capacitor gap for zero-bias voltage. The effective capacitor area is given by A and $\epsilon_0 = 8.85\times 10^{-12}$ C^2/nm^2 is an electrostatic constant. For a given bias voltage, the new equilibrium position is determined from the condition $\partial\mathcal{E}_T/\partial\epsilon = 0$ and the measured effective bending modulus is then

$$y^* \equiv \frac{\partial^2 \mathcal{E}_T}{\partial \epsilon^2}\bigg|_{eq} = y - \left(\frac{\epsilon_0 A}{d_0^3}\right) V_B^2 \left[1 + \frac{3}{2}\left(\frac{\epsilon_0 A V_B^2}{y d_0^3}\right) + \cdots\right]. \qquad (12)$$

In the case of a reed of rectangular cross section, the bending modulus at the end of the reed is related to the Young's modulus along the reed by the expression $E = (4/b)(l/t)^3 y$, where b is the width of the reed. We thus find for the relative change in Young's modulus

$$[E(V) - E(0)]/E(0) = -kV^2(1 + \tfrac{3}{2}kV^2 + \cdots), \qquad (13)$$

where $k = 4\epsilon_0 A l^3/(d_0^3 t^3 bE)$. This modulus correction goes as t^{-3} and thus may be significant for thin samples.

A consideration of the energy dissipation in the receiver bias circuit[20] shows that the change in the internal friction due to the dc bias has the same form as that given in Eq. (13). For the sample dimensions used in this study, the electrostatic

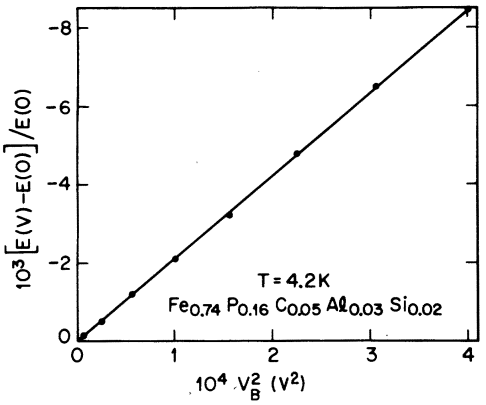

FIG. 3. dc bias effect. The linear behavior of the data indicate that the shift in Young's modulus is proportional to V_B^2, where V_B is the bias voltage. Corrections to the measured modulus can be substantial for very thin reeds. These data were taken with a 4-V-rms driving voltage.

correction to the modulus and internal friction is only important for the fundamental resonance. In Fig. 3 we present measurements at He^4 temperatures for the Young's modulus obtained from the fundamental resonance of an $Fe_{0.74}P_{0.16}C_{0.05}Al_{0.03}Si_{0.02}$ alloy. The relative modulus shift is seen to be proportional to V_B^2 as predicted. The slope of these data, given by the straight line, is consistent with an estimation of the effective capacitor area and gap. Most of the measurements presented here were carried out with a dc bias voltage in the range 5–20 V which leads to an error in the absolute magnitude of the fundamental Young's modulus and internal friction of less than 0.03% and 1%, respectively. These uncertainties are comparable to the resolution of the measurements.

III. RESULTS

A. $Pd_{0.81}Si_{0.19}$

The $Pd_{0.81}Si_{0.19}$ amorphous sample, 100 μm thick, was initially annealed at 570 K for 5 min to remove strains associated with sample preparation. X-ray analysis after the anneal showed no sign of crystallinity. Amorphous measurements at the first and second flexural overtones were carried out and the sample was then crystallized by slowly heating from 600 to 700 K during a 2-h period. Using this procedure, the sample had time to crystalline before reaching the glass transition temperature T_g = 650 K. This minimized bending of the specimen due to low viscosity in the amorphous state near T_g. The clamped sample remained in the copper block during the entire crystallization process. X-ray diffraction analysis of the crystalline phase indicated the presence of Pd (fcc) and Pd_3Si (orthorhombic).

In Fig. 4 we show the temperature dependence of Young's modulus from 1.5–300 K for the amorphous and crystalline phases of $Pd_{0.81}Si_{0.19}$. The data are normalized to the room-temperature values given in Table I. The measurements were taken under equilibrium conditions with the sample holder held a fraction of a degree above the temperature of the surrounding heat shield. The temperature dependence of the amorphous modulus at liquid-helium temperatures indicates the presence of a weak anomaly. Relative changes in the Young's modulus of a part in 10^5 could be detected with the present apparatus. With this high resolution, measurements of velocity dispersion between the first and second overtones were also carried out. Between He^4 and room temperature, we observed a Young's-modulus dispersion of $(V_2 - V_1)/V_1 = 8\times10^{-4}$ and 8.8×10^{-4} for the amorphous and crystalline phases, respectively.

The internal friction at resonant frequencies of $f_1 = 219.6$ Hz and $f_2 = 1354$ Hz are shown in Fig. 5 for amorphous $Pd_{0.81}Si_{0.19}$. These measurements are well below the glass transition temperature of 650 K. At temperatures below ~40 K, the internal friction at the two frequencies are approximately equal and constant. It is interesting to note that over most of the temperature range covered, the internal friction of the second overtone is less than that of the fundamental. These measurements may be compared to the internal friction in the crystallized phase of the same $Pd_{0.81}Si_{0.19}$ sample which is shown in Fig. 6 for the same two flexural overtones. The data for the crystalline phase are similar to the amorphous measurements at low temperatures (below 30 K); however, at higher temperatures the damping of the second overtone in the crystalline phase becomes much larger than the fundamental.

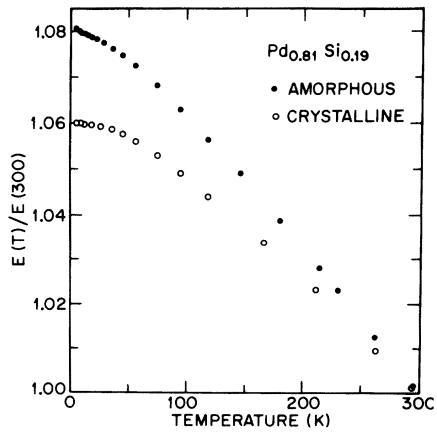

FIG. 4. Temperature dependence of the Young's modulus in $Pd_{0.81}Si_{0.19}$. The solid and open circles represent the amorphous and crystalline phases respectively. At 300 K, the amorphous modulus has the strongest temperature dependence. There is a slight anomaly in the amorphous modulus at liquid-helium temperatures.

TABLE I. Young's modulus and its temperature dependence in the amorphous and crystalline phases of several metallic alloys. The values in parenthesis represent the crystalline phase. The expression $\Delta E/E \equiv (E_c - E_a)/E_a$, where E_a and E_c are the moduli in the amorphous and crystalline phases, respectively.

Alloy	E(0 K) (10^{11} dyn/cm^2)	E(300 K) (10^{11} dyn/cm^2)	$10^4(1/E)(\partial E/\partial T)$ (K^{-1}) at 300 K	$\Delta E/E$ (%) at 300 K
$Pd_{0.81}Si_{0.19}$	8.7[a] (10.7)	8.0[a] (10.1)	−2.6[a] (−2.5)	26
$Fe_{0.74}P_{0.16}C_{0.05}Al_{0.03}Si_{0.02}$	9.1 (12.0)	8.5 (11.4)	−2.8 (−2.0)	34
$Ni_{0.74}P_{0.16}B_{0.07}Al_{0.03}$	9.4 (12.7)	8.6 (12.0)	−3.4 (−2.7)	39
$Ni_{0.76}P_{0.24}$		10.0 (13.8)		34
$Fe_{0.75}P_{0.16}Si_{0.06}Al_{0.03}$	10.6	9.9	−2.6	
$Ni_{0.33}Pd_{0.47}P_{0.20}$		7.6		
$Fe_{0.32}Pd_{0.48}P_{0.20}$		7.9		

[a]Results for an annealed amorphous sample.

B. Multicomponent alloys

Acoustic measurements were also carried out on the multicomponent metallic alloys $Fe_{0.74}P_{0.16}C_{0.05}Al_{0.03}Si_{0.02}$ (designated Fe-I), $Fe_{0.75}P_{0.16}Si_{0.06}Al_{0.03}$ (Fe-II) and $Ni_{0.74}P_{0.16}B_{0.07}Al_{0.03}$ (Ni-I). The iron alloys Fe-I and Fe-II were ferromagnetic in the temperature range studied with Curie temperatures of 598 and 602 K, respectively. The internal friction of initially quenched amorphous samples of the three alloys is shown in Fig. 7. These data correspond to the fundamental resonance of reeds, 45 μm thick. Several days were required to obtain each set of data due to the wide temperature range covered. All the multicomponent alloys investigated exhibit a broad low-temperature internal-friction anomaly in the range 1.5–80 K.

The low-temperature anomaly was investigated in more detail for the alloy Fe-I. Low-temperature measurements were initially carried out on the amorphous Fe-I sample and then repeated after an annealing at 670 K for 8 min. X-ray analysis of the annealed sample, which remained in the copper housing, showed it to be amorphous. The sample was then crystallized by heating from 600 to 800 K over a 2-h period. X-ray diffraction analysis of the crystallized sample confirmed the presence of Fe (bcc), Fe_2P (hexagonal), and Fe_3P (tetragonal). Visual observation of the sample also indicated the existence of precipitated carbon. A comparison of the amorphous, annealed, and crystalline measurements at low temperatures is shown in Fig. 8. The amorphous and annealed measurements show a broad maximum centered near 20 K. In the case of the crystalline measurements, the internal-friction maximum is much sharper and is shifted up in temperature to ~24 K. The absolute magnitude of the internal friction is seen to decrease as the sample is progressively heat treated at higher temperatures.

A Young's-modulus dispersion also accompanied the internal-friction maximum observed in the amorphous state of Fe-I, Fe-II and Ni-I. This can be seen in Fig. 9, which shows the Young's-modulus temperature dependence of Fe-I after various stages of heat treatment. The main effect of annealing the amorphous sample is to decrease the low-temperature Young's modulus relative to its value at 300 K.

IV. DISCUSSION

A. Young's modulus

From the measurements of Young's modulus as a function of temperature, we have obtained $E(T = 300\ \text{K})$, $E(T = 0\ \text{K})$ and $(1/E)(\partial E/\partial T)$. These values for the various alloys measured are given in Table I. Also presented in this table are the changes in the modulus upon crystallization evaluated at 300 K. The changes in modulus at $T = 0$ K is generally 2%-3% less than the room-temperature value. In all the investigated alloys, crystallization reduced the temperature dependence of Young's

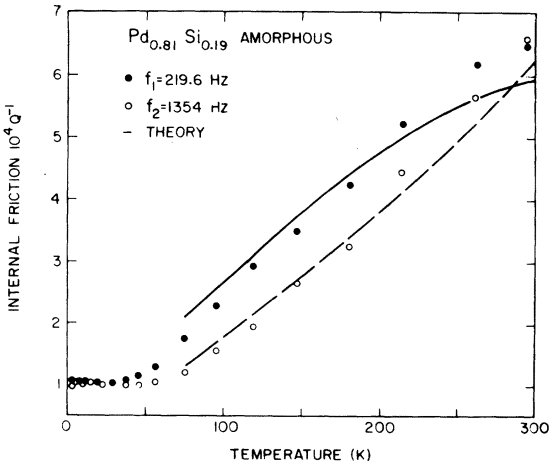

FIG. 5. Temperature dependence of the internal friction in amorphous $Pd_{0.81}Si_{0.19}$. The solid and dashed curves correspond to the calculated thermoelastic relaxation for the first and second overtones, respectively. The internal friction at the two frequencies becomes equal at the temperature ($T = 285$ K) calculated from the thermoelastic process; however, the magnitude of the experimental loss is larger. The frequencies given in the figure represent room-temperature values.

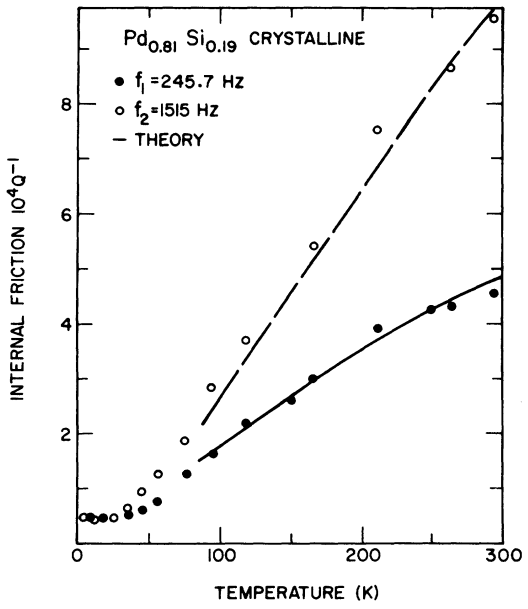

FIG. 6. Temperature dependence of the internal friction in crystalline $Pd_{0.81}Si_{0.19}$. The calculated thermoelastic relaxation for the first and second overtones is represented by the solid and dashed curves, respectively.

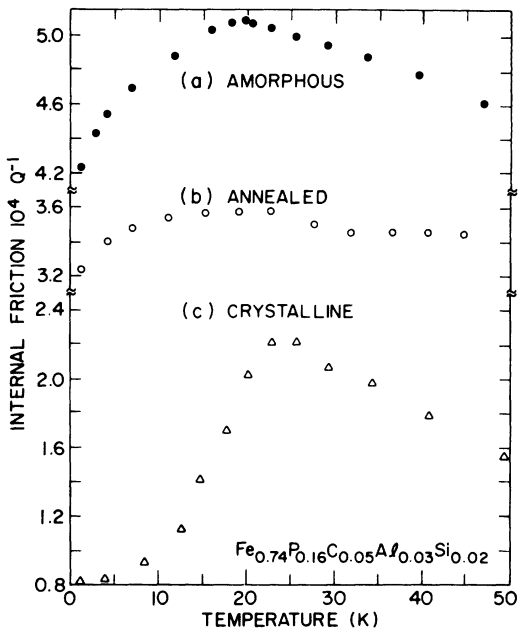

FIG. 8. Temperature dependence of the internal friction in $Fe_{0.74}P_{0.16}C_{0.05}Al_{0.03}Si_{0.02}$ in the range 1.5–50 K. (a) The solid circles represent measurements of the initially quenched amorphous sample. (b) The open circles were taken after annealing the amorphous sample at 670 K for 8 min. (c) After crystallization, the measurements were repeated and are shown by the open triangles. The magnitude of the internal friction decreases with successive heat treatments.

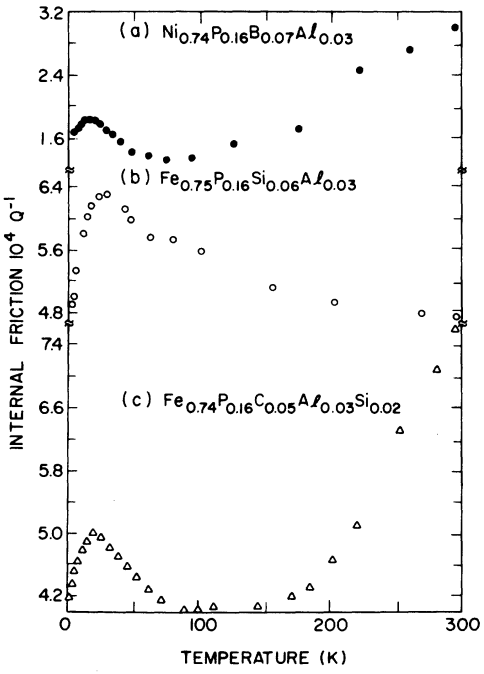

FIG. 7. Temperature dependence of the damping in the amorphous phase of multicomponent iron and nickel alloys in the range 1.5–300 K. All the alloys show a broad low-temperature internal-friction maximum. The fundamental flexural frequencies at 300 K are (a) f_1=129.2 Hz, (b) f_1=138.7 Hz, and (c) f_1=154.9 Hz.

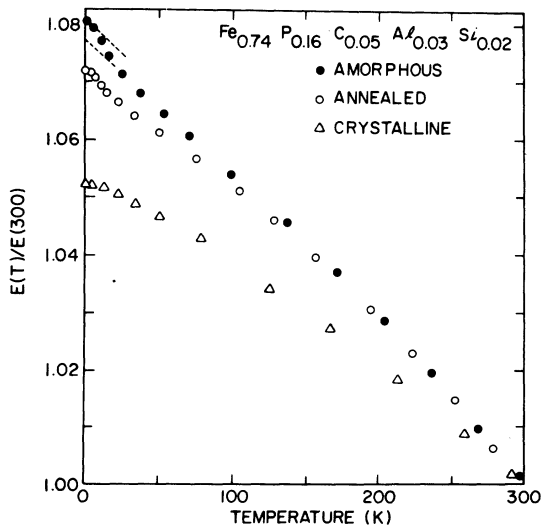

FIG. 9. Temperature dependence of Young's modulus of the fundamental flexural resonance in $Fe_{0.74}P_{0.16}C_{0.05}Al_{0.03}Si_{0.02}$. The solid and open circles represent measurements in the initially quenched and annealed samples, respectively. The crystalline measurements are given by the open triangles. The dashed lines are an estimate of the dispersion associated with the low-temperature internal-friction maximum. The resonant frequencies at 300 K are (●) 154.9 Hz, (○) 156.5 Hz, and (△) 179.0 Hz.

modulus at 300 K. In the case of $Pd_{0.81}Si_{0.19}$, the 26% modulus change upon crystallization agrees with earlier measurements.[5,9] The temperature dependence of the amorphous and crystalline Young's modulus is also in accord with the room-temperature dynamic measurements of Ref. 9. However, the temperature dependence of the amorphous modulus is a factor of 2.5 smaller than the results of static measurements.[5] This large discrepancy between the static and dynamic measurements cannot be accounted for by the small difference between the adiabatic and isothermal moduli.[21] In the early stages of this investigation, room-temperature Young's-modulus measurements were performed on metallic alloys with compositions $Ni_{0.76}P_{0.24}$, $Ni_{0.33}Pd_{0.47}P_{0.20}$, and $Fe_{0.32}Pd_{0.48}P_{0.20}$. The results for these alloys are also presented in Table I. For these measurements, the uncertainty in the modulus is approximately 15%. All the modulus changes $(E_c - E_a)/E_a$ given in Table I lie within the theoretical estimated limits of 21%-43%. An alternate estimate of the modulus change between the amorphous and crystalline phases may be obtained from a consideration of the dependence of the elastic moduli on strain energy. This approach does not depend on specific microscopic models such as those used by Weaire *et al.*[16] Zener[22] has derived an approximate expression relating the strain dependence of the shear modulus to its temperature dependence. Since Young's modulus is linearly related to the shear modulus for a constant Poisson's ratio, we obtain

$$\frac{dE}{E} = \left[\left(\tfrac{3}{2} NkE\right)^{-1} \left(\frac{dE}{dT}\right) \right] d\epsilon, \tag{14}$$

where N is the total number of molecules, k is Boltzmann's constant, and ϵ is the strain energy. From measurements of the heat of crystallization,[23] we take $\epsilon \simeq 1.5$ kcal/mole and use a typical value $E^{-1}(dE/dT) = 2.8\times10^{-4}$ K^{-1} obtained from Table I. This leads to a Young's-modulus change of 14%. This low value does not take into account the effects of internal displacements, which have been shown[16] to introduce a large additional change in the modulus.

B. Internal friction

The internal-friction measurements are discussed in terms of two relaxation processes. Thermoelastic relaxation is shown to be the main contribution to the internal friction at high temperatures (100–300 K). At lower temperatures, thermoelastic relaxation approaches zero as $T \to 0$ K. In the low-temperature regime (1.5–100 K), the iron and nickel alloys exhibit an internal-friction anomaly which is shown to be consistent with a relaxation process containing a very broad spectrum of relaxation times.

1. $Pd_{0.81}Si_{0.19}$

In the case of $Pd_{0.81}Si_{0.19}$, which does not show a measurable low-temperature anomaly, we assume the internal friction may be described by a single relaxation process given by Eqs. (2) and (3). In Fig. 5, the essentially constant amorphous internal friction at low temperature was assumed to be a clamping loss and was removed from the higher-temperature measurements to obtain the intrinsic sample loss at each frequency. The relaxation time for the process may be estimated from the ratio of the internal friction at the two frequencies

$$\frac{Q_2^{-1}}{Q_1^{-1}} = \left(\frac{\omega_2}{\omega_1}\right) \frac{1+\omega_1^2\tau^2}{1+\omega_2^2\tau^2}. \tag{15}$$

This procedure yields a relaxation time which increase with decreasing temperature and has the value 2.8×10^{-4} and 4.8×10^{-4} sec at 300 and 100 K, respectively. We associate this relaxation time with the thermoelastic process. From Eq. (1) we obtain a room-temperature diffusivity $D = 0.039$ cm^2 sec^{-1}, which is ~20% smaller than the value reported by Berry.[9,24]

In order to directly compare the thermoelastic theory to the measurements, we make the simplifying assumption that the amorphous alloy may be represented by a Debye solid. Furthermore, we assume the expansion coefficient is linearly related to the specific heat through the Grüneisen expression[25]

$$\alpha = \frac{\gamma\kappa}{3v} C_v \tag{16}$$

where γ is the Grüneisen constant, κ is the compressibility, and v is the specific volume. A Debye temperature of 300 K was used to calculate the specific heat and κ was obtained from recent ultrasonic measurements.[7] The theory was normalized to the first-overtone amorphous data at 200 K by setting the Grüneisen constant $\gamma = 2.6$. The solid and dashed curves shown in Fig. 5 correspond to the predictions of the thermoelastic theory for the first and second overtones, respectively. In the range 100–300 K, $\omega_1\tau \simeq 0.5$ while $\omega_2\tau \simeq 3$. This accounts for the fact that $Q_2^{-1} \lesssim Q_1^{-1}$ over most of this temperature range. Experimentally, $Q_2^{-1} = Q_1^{-1}$ at ~285 K, which is the same crossover temperature calculated from the thermoelastic process. There is sufficient agreement between theory and experiment to conclude that the thermoelastic process is the dominant loss mechanism in amorphous $Pd_{0.81}Si_{0.19}$ at these frequencies. The analysis was carried a step further to estimate the thermal conductivity λ. Derived values for D and λ are given in Table II. The amorphous thermal conductivity

TABLE II. Estimated diffusivity and thermal conductivity of $Pd_{0.81}Si_{0.19}$.

Phase	Diffusivity D ($cm^2\,sec^{-1}$) 100 K	300 K	Conductivity λ ($W\,cm^{-1}\,K^{-1}$) 100 K	300 K
Amorphous	0.023	0.039	0.043	0.11
Crystalline	0.060	0.075	0.11	0.20

decreases monotonically with decreasing temperature as has been observed in other nonmetallic amorphous materials.[26] However, the metallic amorphous conductivities are one to two orders of magnitude larger than their nonmetallic counterparts, due to a large electronic contribution. The measured room-temperature amorphous conductivity $\lambda = 0.11\ W\,cm^{-1}K^{-1}$ is ~20% less than the value reported by Berry and Pritchet.[9]

A similar comparison between theory and experiment was carried out for the crystalline data in Fig. 6. The solid and dashed lines are again the theoretical predictions using a Debye temperature of 300 K and a normalized Grüneisen constant of 2.7. The theoretical fit is much better in the crystalline phase than the amorphous phase. This may be accounted for by introducing an additional amorphous loss mechanism, which is associated with the glass transition and is not negligible at room temperature. This may also explain the origin of the excess dispersion obtained at room temperature, which is ~30% greater than the thermoelastic prediction. Some evidence confirming pretransitional acoustic loss in $Pd_{0.80}Si_{0.20}$ has been reported.[27] However, more-precise high-temperature measurements are needed to quantitatively describe this process. From Table II we see that the diffusivity and conductivity in the crystalline phase of $Pd_{0.81}Si_{0.19}$ are approximately twice their amorphous values.

2. *Fe and Ni alloys*

The iron and nickel alloys investigated, all exhibited a low-temperature acoustic anomaly in both the amorphous and crystalline states. Above 100 K, measurements of the second-overtone damping (not shown in Fig. 7 for clarity) had a larger magnitude and temperature dependence than the fundamental for all samples investigated. We assume that the internal friction measured above ~100 K was primarily due to thermoelastic relaxation as was the case for $Pd_{0.81}Si_{0.19}$. A quantitative comparison between theory and experiment could not be made because of the large uncertainty in determining the background clamping loss. However, it is clear from Fig. 7 that the diffusivity and conductivity are strong functions of the alloy composition, if we assume the entire high-temperature internal friction is due to the thermoelastic effect. Near room temperature an additional contribution may arise from the diffusion of boron or carbon, as has been reported for low-carbon steel.[28]

In the temperature range 1.5–80 K the internal-friction measurements at the second overtone revealed the same temperature dependence as the fundamental resonances shown in Fig. 7. The absolute magnitude of the second-overtone damping was also essentially the same as the fundamental in this range. A relaxation process or hysteresis loss mechanism may account for low-temperature damping which is approximately independent of frequency. Hysteresis losses are usually amplitude dependent, while relaxation processes are not. Thus to distinguish between these processes, measurements of the amplitude dependence of the damping were carried out. In Fig. 10, we show the strain dependence of the first and second overtones of amorphous Fe-II. These data correspond to strains in the range of 8×10^{-8} to 8×10^{-6}. Within the scatter, the internal friction is independent of strain.

The low-temperature measurements were analyzed assuming a thermally activated relaxation mechanism was responsible for the observed internal friction. For this process, the relaxation time τ has the form

$$\tau = \tau_0 e^{H/kT}, \tag{17}$$

where H is the activation energy and k is Boltzmann's constant. The prefactor may be estimated by assuming $\tau_0 = \hbar/(kT_M)$, where T_M is the temperature of the internal-friction maximum and $\hbar = h/2\pi$, with h being Planck's constant. The amorphous specimens of Fe-I, Fe-II, and Ni-I have internal-friction maxima at 20, 29, and 16 K, respectively. The most accurate and detailed measurements were

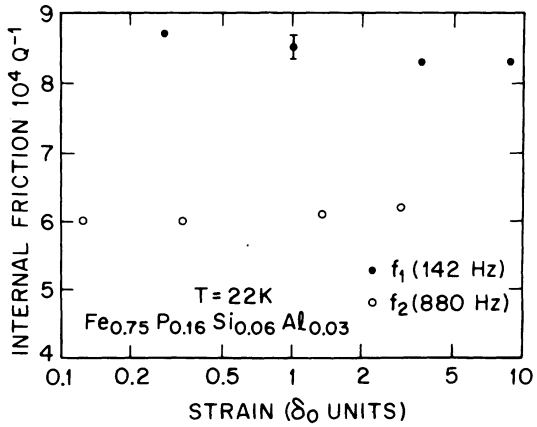

FIG. 10. Strain dependence of the internal friction near its maximum in $Fe_{0.75}P_{0.16}Si_{0.06}Al_{0.03}$. The strains are in units of $\delta_0 = 7.8\times10^{-7}$. Within the experimental uncertainty, the low-temperature internal friction is independent of strain for $10^{-7} \lesssim \delta \lesssim 10^{-5}$.

carried out on Fe-I samples and we will thus present a complete analysis of the internal friction in this alloy.

For a thermally activated process with a single relaxation time, the normalized internal friction may be expressed in the form

$$Q^{-1}/Q_M^{-1} = \mathrm{sech}[(-H/k)(T_M^{-1} - T^{-1})] \qquad (18)$$

where Q_M^{-1} is the maximum value of the damping. A plot of Q^{-1}/Q_M^{-1} vs $(T_M^{-1} - T^{-1})$ for a single relaxation process yields a symmetric curve about $T = T_M$ with a width that depends on the activation energy. Using the fact that $\omega\tau = 1$ at the peak temperature, and Eq. (17), we obtain $H = 850$ cal/mole as an estimate for the activation energy of the Fe-I alloy. A similar analysis of the internal friction in Fe-II and Ni-I yields the activation energies $H = 1270$ and 680 cal/mole, respectively. These activation values imply that the internal-friction maximum of the fundamental and second overtone differ in temperature by only 1.4–2.4 K. These temperature differences could not be resolved in the present experiment due to scatter in the data; however, they are consistent with the measurements.

In Fig. 11 we present the normalized internal friction of amorphous Fe-I as a function of $T_M^{-1} - T^{-1}$. The expected behavior of a single relaxation process with $H = 850$ cal/mole is also shown by the solid line. The data exhibit a broad asymmetry relative to $T = T_M$ with a large tail at low temperatures.[29] It is clear that the measurements are not represented by a single relaxation time, but require a broad asymmetric distribution of τ's. To estimate the magnitude of the distribution, we have assumed a log-normal distribution of relaxation times, as discussed in Sec. I, and used the analysis method proposed by Norwick and Berry.[30] The dashed curve in Fig. 11 represents a log-normal distribution with $\beta = 15$ and fits the high-temperature data. Since the log-normal distribution is symmetric, it cannot account for the low-temperature asymmetry.[31] This value of β leads to a relaxation strength $[E(\omega = \infty) - E(\omega = 0)]/E(\omega = 0) \simeq 1.6 \times 10^{-3}$, which may be compared to the measured dispersion in the amorphous Young's modulus $\Delta E/E \approx 3 \times 10^{-3}$, shown by the dashed line in Fig. 9.[32] Low-temperature measurements of the internal friction in crystallized Fe-I, shown in Fig. 8, have also been compared to a log-normal distribution. These results are given in Fig. 12, where the dashed curve represents $\beta = 13$ and $H = 1050$ cal/mole. The crystallized data fit a log-normal distribution reasonably well for $T \gtrsim T_M$. Only a small remnant of the low-temperature amorphous tail remains. We conclude that the low-temperature tail of the distribution of relaxation times is an intrinsic property of the amorphous state. This asymmetric behavior in the relaxation spectrum has also been observed in aluminosilicate glasses[12] and sheet glass.[33]

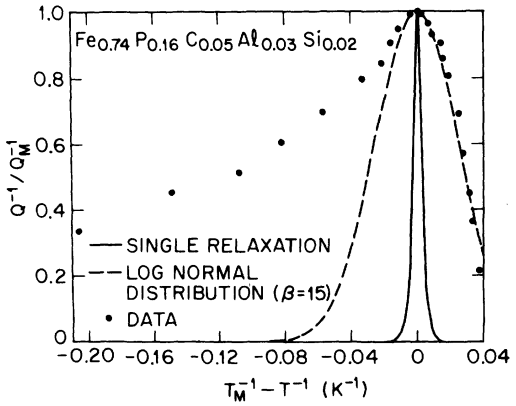

FIG. 11. Normalized internal friction versus the inverse temperature for amorphous $Fe_{0.74}P_{0.16}C_{0.05}Al_{0.03}Si_{0.02}$. The solid curve represents a single relaxation process with an activation energy $H = 850$ cal/mole. The dashed curve corresponds to a symmetric log-normal distribution of relaxation times with $\beta = 15$ and $H = 850$ cal/mole. The data exhibit a large asymmetry in the low-temperature regime. Different choices of the background internal friction affect the magnitude of the asymmetry; however, a large low-temperature tail prevails for all reasonable values of the background.

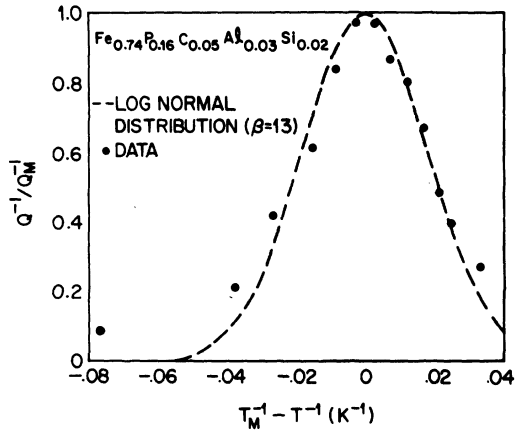

FIG. 12. Normalized internal friction versus the inverse temperature for crystalline $Fe_{0.74}P_{0.16}C_{0.05}Al_{0.03}Si_{0.02}$. The dashed curve corresponds to a lognormal distribution with $\beta = 13$ and $H = 1050$ cal/mole. Only a small remnant remains of the low-temperature amorphous tail.

The most consistent interpretation of low-temperature acoustic behavior in pure glass-forming materials is based on oscillations of atoms in an open tetrahedrally coordinated structure. Anderson and Bömmel[34] concluded that the relaxation process responsible for their ultrasonic loss in fused silica was due to transverse motion of oxygen atoms between two or more equivalent sites. This

approach has been modified more recently, by Vukcevich[35] whose model gives better agreement with the measured oxygen angle distribution. These and other explanations for silica-like glasses are generally based on an open structure with specific bonding properties and are probably not suited to metallic glasses, which have a close-packed structure with nondirectional bonding.

Recently, Scott and MacCrone[36] carried out low-frequency vibrating-reed measurements in silica glasses, which revealed relaxation processes at low temperatures similar to the present results. To explain their data, they assumed that amorphous materials contain local combinations of atoms which vibrate as an almost-independent Einstein oscillator with frequency ω_0. These low-frequency vibrational modes, which are in excess of the usual Debye spectrum, couple to the strain through a Grüneisen constant. This coupling leads to anelastic relaxation, which was found to be consistent with their kHz measurements.

The relaxation strength for this process is

$$\Delta \equiv [E(\omega=\infty) - E(\omega=0)]/E(\omega=0)$$

$$= (\alpha_E \gamma_E \hbar\omega_0/2k)F(z), \qquad (19)$$

where α_E and γ_E are the thermal expansion and Grüneisen constant associated with the Einstein oscillators of frequency ω_0, and $F(z) = (e^z - 2z - e^{-z})/z^2$ with $z = \hbar\omega_0/kT$. The function $F(z) \to 0$ at high temperature ($T \gg T_M$) and diverges as $T \to 0$. Since α_E is assumed to approach zero at low temperatures, the relaxation strength is expected to to be small at high temperatures ($T > T_M$) and increase with decreasing temperature to some limiting value. For $z = 1$ ($T = T_M$), the relaxation strength is given by $\Delta = 0.175\alpha_E\gamma_E T_M$. Setting $\alpha_E \simeq 10^{-5}$ K^{-1}, $\gamma_E \simeq 2.7$, and $T_M = 20$ K, we obtain the rough estimate $\Delta(T = T_M) \approx 10^{-4}$. This gives an order-of-magnitude agreement with the measured velocity dispersion at the internal-friction maximum. The enhancement of the relaxation strength at temperatures below T_M may also explain the asymmetric damping and dispersion observed experimentally in the low-temperature regime ($T < T_M$). A more accurate determination of the parameters in this theory is necessary before a quantitative test of its predictions can be carried out.

Finally, we must mention a recent theoretical model,[37,38] introduced to explain the behavior of glasses at low temperatures ($T \lesssim 1$ K). In this approach, a glass is assumed to contain a distribution of tunneling states, each consisting of a group of atoms having two equilibrium positions in an asymmetric double well potential. The assumption of a uniform energy distribution of these states leads to a linear temperature dependence of the specific heat. The theory also predicts a resonant absorption of phonon energy which leads to a saturation effect at high frequencies. Both of these effects have been observed experimentally.[26,39,40] At higher temperatures, relaxation processes become more important than resonant absorption. Recently, attenuation measurements[41] in As_2S_3 from 1.5 to 300 K were explained by the tunneling approach using a phenomenological energy distribution function. Further development of this theory, which is an alternative to the Einstein oscillator approach, may ultimately describe the low-temperature acoustic behavior reported in this paper.

V. CONCLUSION

We have shown that thermoelastic relaxation is the major loss mechanism in reeds of metallic glass in the temperature range 100–300 K. In $Pd_{0.81}Si_{0.19}$, the comparison of the internal-friction measurements to the thermoelastic relaxation theory yields information regarding the magnitude and temperature dependence of the thermal conductivity and diffusivity. A broad low-temperature internal-friction maximum and Young's-modulus dispersion is observed in iron and nickel alloys. Even in $Pd_{0.81}Si_{0.19}$, there appears to be a small Young's-modulus dispersion effect at liquid-helium temperatures (see Fig. 4). Since these measurements were carried out in an annealed amorphous sample, it is quite possible that an initially quenched Pd-Si alloy would reveal a more pronounced low-temperature anomaly. Recent MHz ultrasonic measurements[8] in Pd-Si alloys also show a broad low-temperature attenuation maximum. The magnitude of the low-temperature internal friction in the multicomponent alloys is independent of strain amplitudes in the range 10^{-7}–10^{-5}. In $Fe_{0.74}P_{0.16}C_{0.05}Al_{0.03}Si_{0.02}$, the distribution of thermally activated relaxation times is very broad and asymmetric. This asymmetry is removed upon crystallization and it appears to be a property of the amorphous phase. The coupling of localized atomic arrangements to the bulk through a Grüneisen parameter, proposed by Scott and MacCrone, leads to a temperature-dependent relaxation strength, which may account for the asymmetry observed in the internal friction and Young's modulus. More quantitative conclusions regarding these low-temperature anomalies must await further investigation, particularly at higher frequencies.

The Young's modulus of several metallic alloys was measured from 1.5 to 300 K. At 300 K the temperature dependence of the modulus in both the amorphous and crystalline phases was linear with values in the range $(1/E)(\partial E/\partial T) \approx (2\text{–}3.4) \times 10^{-4}$ K^{-1}. The amorphous temperature dependence was always greater than the crystalline. All the alloys

exhibited a softening of Young's modulus in the amorphous phase. Crystallization of the amorphous samples resulted in a large increase in the modulus ranging from 26% to 39% at 300 K. At $T = 0$ K the change upon crystallization was smaller by 2%–3%.

ACKNOWLEDGMENTS

We are indepted to Brage Golding, P. C. Hohenberg, and J. B. Lastovka for many helpful discussions. We also acknowledge the technical assistance of V. G. Chirba.

[1]Pol Duwez, Trans. Am. Soc. Met. 60, 605 (1967).
[2]B. C. Giessen and C. N. J. Wagner, in *Physics and Chemistry of Liquid Metals*, edited by S. Z. Beer (Dekker, New York, 1972), p. 633; and H. S. Chen and C. E. Miller, Rev. Sci. Instrum. 41, 1237 (1970).
[3]S. Jovanovec and C. S. Smith, J. Appl. Phys. 32, 121 (1961).
[4]M. F. Ashby, A. N. Nelson, and R. M. A. Centamore, Scr. Metall. 4, 715 (1970).
[5]T. Masumoto and R. Maddin, Acta Metall. 19, 725 (1971).
[6]H. S. Chen, H. J. Leamy, and M. Barmatz, J. Non-Cryst. Solids 5, 444 (1971).
[7]Brage Golding, B. G. Bagley, and F. S. L. Hsu, Phys. Rev. Lett. 29, 68 (1972).
[8]M. Dutoit and H. S. Chen, Appl. Phys. Lett. 23, 357 (1973).
[9]B. S. Berry and W. C. Pritchet, J. Appl. Phys. 44, 3122 (1973).
[10]L. R. Testardi, J. T. Krause, and H. S. Chen, Phys. Rev. B 8, 4464 (1973).
[11]C. Zener, Phys. Rev. 52, 230 (1937); and Phys. Rev. 53, 90 (1938).
[12]M. Barmatz and Brage Golding, Phys. Rev. B 9, 3064 (1974).
[13]D. W. Moore and D. E. Day, Phys. Chem. Glasses 12, 75 (1971).
[14]W. A. Yager, Physics 7, 434 (1936).
[15]A. S. Norwick and B. S. Berry, IBM J. Res. Dev. 5, 297 (1961).
[16]D. Weaire, M. F. Ashby, J. Logan, and M. J. Weins, Acta Metall. 19, 779 (1971).
[17]The Ni-P alloy, prepared by an electrodeposition technique, was obtained from Dr. J. Logan.
[18]M. Barmatz, H. J. Leamy, and H. S. Chen, Rev. Sci. Instrum. 42, 885 (1971).
[19]S. Timoschenko, in *Vibration Problems in Engineering*, 3rd ed. (Van Nostrand, Princeton, N. J., 1955), p. 338.
[20]L. R. Testardi (private communication).
[21]The difference between the adiabatic and isothermal Young's modulus is $(E_S - E_T)/E_T = TE_T\alpha^2/C_p$. At 300 K, this difference is less than 1%.
[22]C. Zener, Acta Crystallogr. 2, 163 (1949).
[23]H. S. Chen and D. E. Polk (unpublished); and H. S. Chen, J. Non-Cryst. Solids 12, 333 (1973). We have estimated the strain energy ϵ from experiments, which provide only partial heats of crystallization.
[24]B. S. Berry, in *Anelastic Relaxation in Crystalline Solids* (Academic, New York, 1972) p. 502.
[25]In these calculations, we have replaced the specific heat C_v by C_p. This corresponds to an error of less than 1% over the experimental temperature range.
[26]R. C. Zeller and R. O. Pohl, Phys. Rev. B 4, 2029 (1971).
[27]A. Eisenberg and S. Reich, in *Amorphous Materials* (Wiley-Interscience, New York, 1972), p. 79.
[28]See, for example, C. Wert and C. Zener, Phys. Rev. 76, 1169 (1949).
[29]The degree of the asymmetry varies somewhat with the choice of the background internal friction. However, all reasonable values of the background led to a large low-temperature tail.
[30]A. S. Norwick and B. S. Berry, IBM J. Res. Dev. 5, 312 (1961).
[31]A reduction in the asymmetry at low temperatures is obtained by assuming a power-law form for the relaxation time, $\tau = \tau_0 T^{-a}$, where a is a positive integer. However, at this time there is no theoretical justification for using this form.
[32]Most of the measured dispersion occurs for $T < T_M$ and is associated with the long tail in the relaxation distribution, which is not accounted for by the log-normal distribution. The crystalline phase does not exhibit an asymmetric distribution and the measured dispersion is less apparent.
[33]G. J. Copley and D. R. Oakley, Phys. Chem. Glasses 9, 141 (1968).
[34]O. L. Anderson and H. E. Bömmel, J. Ceramic Soc. 38, 125 (1955).
[35]M. R. Vukcevich, J. Non-Cryst. Solids, 11, 25 (1972).
[36]W. W. Scott and R. K. MacCrone, Phys. Rev. B 1, 3515 (1970); and S. Muller, III, M. Tomozawa, and R. K. MacCrone, *Amorphous Materials* (Wiley-Interscience, New York, 1972), p. 89.
[37]P. W. Anderson, B. I. Halperin, and C. M. Varma, Philos. Mag. 25, 1 (1972).
[38]W. A. Phillips, J. Low Temp. Phys. 7, 351 (1972).
[39]R. B. Stephens, Phys. Rev. B 8, 2896 (1973).
[40]S. Hunklinger, W. Arnold, St. Stein, and R. Dransfeld, Phys. Lett. A 42, 253 (1972); and B. Golding, J. E. Graebner, B. I. Halperin, and R. J. Schutz, Phys. Rev. Lett. 30, 223 (1973).
[41]D. Ng and R. J. Sladek, Proceedings of Fifth International Conference on Amorphous and Liquid Semiconductors (1973) (unpublished).